ARTICLE

Magnetic-Bottle and Velocity-Map Imaging Photoelectron Spectroscopy of APS^- (A=$C_{14}H_{10}$ or Anthracene): Electron Structure, Spin-Orbit Coupling of $APS^\bullet$, and Dipole-Bound State of APS^-†

Qin-qin Yuan[a,b,c‡], Zheng Yang[a], Ren-zhong Li[a‡], Wesley J. Transue[d], Zhi-peng Li[a‡], Ling Jiang[b], Niranjan Govind[e], Christopher C. Cummins[d*], Xue-Bin Wang[a*]

a. Physical Sciences Division, Pacific Northwest National Laboratory, 902 Battelle Boulevard, P. O. Box 999, MS K8-88, Richland, Washington 99352, USA
b. State Key Laboratory of Molecular Reaction Dynamics, Dalian Institute of Chemical Physics, Chinese Academy of Sciences, Dalian 116023, China
c. University of Chinese Academy of Sciences, Beijing 100049, China
d. Department of Chemistry, Massachusetts Institute of Technology, Cambridge, MA 02139, USA
e. Environmental Molecular Sciences Laboratory, Pacific Northwest National Laboratory, P. O. Box 999, MS K8-91, Richland WA 99352, USA

(Dated: Received on May 24, 2018; Accepted on June 7, 2018)

Gaseous dibenzo-7-phosphanorbornadiene P-sulfide anions APS^- (A=$C_{14}H_{10}$ or anthracene) were generated via electrospray ionization, and characterized by magnetic-bottle photoelectron spectroscopy, velocity-map imaging (VMI) photoelectron spectroscopy, and quantum chemical calculations. The electron affinity (EA) and spin-orbit (SO) splitting of the $APS^\bullet$ radical are determined from the photoelectron spectra and Franck-Condon factor simulations to be EA=(2.62±0.05) eV and SO splitting=(43±7) meV. VMI photoelectron images show strong and sharp peaks near the detachment threshold with an identical electron kinetic energy (eKE) of 17.9 meV at three different detachment wavelengths, which are therefore assigned to autodetachment from dipole-bound anion states. The B3LYP/6-31++G(d,p) calculations indicate $APS^\bullet$ has a dipole moment of 3.31 Debye, large enough to support a dipole-bound electron.

Key words: Dibenzo-7-phosphanorbornadiene P-sulfide, Electronic structure, Spin-orbit coupling, Dipole-bound state, VMI photoelectron spectroscopy

I. INTRODUCTION

The new synthetic routes that allowed bulk preparation and isolation of 2-phosphaethynolate PCO^- reported in 2011−2013 [1–3] have led to a series of important discoveries that have demonstrated PCO^- as a versatile phosphide-transfer reagent [4, 5], an important precursor to organophosphorus compounds [6–8], and to phosphorus-containing heterocycles [9–13]. Recently, there has been considerable interest in synthesizing dibenzo-7-phosphanorbornadiene compounds, RPA (A=$C_{14}H_{10}$ or anthracene) as potential organic phosphorus precursor molecules for the phosphorus transformation that allow clean generation of phosphorus-related small molecules via anthracene elimination at mild temperatures [14–20]. This strategy has led to successful syntheses of novel inorganic aromatic molecules such as $P_2N_3^-$ [15] and $HCPN_3^-$ [19], as well as an astrophysically interesting species HCP [19]. The electronic structures of $HCPN_3^-$ and $P_2N_3^-$ have been subsequently investigated using gas phase negative ion photoelectron spectroscopy (NIPES) coupled with an electrospray ionization source (ESI) [21, 22].

The PS^- anion along with its neutral radical $PS^\bullet$ and cation PS^+ have been proposed to be important species in astrophysics and astrochemistry [23], and have been a subject of theoretical studies [24] since the first $PS^\bullet$ identification was reported by Dressler and Miescher in 1955 [25]. For the past six decades, only a very limited number of experiments on $PS^\bullet$ and cation PS^+ have been performed [26, 27], but experimental identification of PS^- has yet remained elusive. In this work, we predicted dibenzo-7-phosphanorbornadiene P-sulfide (APS^-) to be a potential source to generate the long sought PS^- anion via anthracene elimination, and to obtain the electronic structures of PS^- and $PS^\bullet$ through NIPES. Upon spraying equimolar so-

†Part of the special issue for celebration of "the 60th Anniversary of University of Science and Technology of China and the 30th Anniversary of Chinese Journal of Chemical Physics".
‡Visiting students supported via PNNL alternate sponsored fellowship program.
*Authors to whom correspondence should be addressed.
E-mail: xuebin.wang@pnnl.gov, ccummins@mit.edu

lutions of APSH and methylenetriphenylphosphorane $Ph_3P{=}CH_2$, we indeed observed an anion species with m/z corresponding to PS^-. However, the subsequent NIPE spectra proved this species was actually PO_2^- [28], presumably due to its oxidation by adventitious O_2 during ESI. The exact reason of missing PS^- under the current procedure is not clear at this point, and remains an interesting subject for future study. During the ESI process, we instead observed abundant intact APS^- anions.

Although the geometries of RPA compounds have been examined by X-ray crystallography [16, 18–20], the intrinsic electronic structure and geometry of gas-phase APS^- have not been studied, though they are the key molecular properties for fundamental understanding of the bond breaking and forming in producing small molecules via anthracene elimination. Therefore, we carried out a joint NIPES [29], velocity-map imaging photoelectron spectroscopy (VMI-PES) [30], and computational study of APS^-, and report our findings in this paper. Photoelectron spectra of APS^- obtained at various laser wavelengths show multiple spectral bands representing electronic transitions from the ground state of APS^- to the ground and excited states of neutral $APS^\bullet$. With the aid of quantum chemical computations and Franck-Condon factor (FCF) simulations, electron affinity (EA) and spin-orbit (SO) splitting of $APS^\bullet$ are determined. VMI photoelectron spectroscopy exhibits sharp peaks near the detachment threshold with an identical electron kinetic energy (eKE) of 17.9 meV using three different laser wavelengths (440, 450, and 460 nm) — a direct indication of observation of dipole-bound states in the APS^- anion. The existence of dipole bound states was also confirmed by the calculated dipole-bound electron orbitals.

II. EXPERIMENTS

The experiments were carried out using PNNL ESI-NIPES [29] and VMI-PES [30]. 0.1 mmol/L equimolar solutions of APSH and methylenetriphenylphosphorane $Ph_3P{=}CH_2$ dissolved in dry acetonitrile solvent, were prepared in a N_2 glovebox and used for electrospray. The preparation and properties of the molecule HP(S)A will be reported in an upcoming publication. The produced APS^- ions were transported by quadrupole ion guides, and directed by a 90° bender into the cryogenic 3D ion trap (set at 20 K) where they were accumulated and cooled for 20−100 ms by collisions with cold buffer gas (20% H_2 balanced in helium). The cooling of the anions to 20 K eliminated possible extra features due to vibrational hot bands and improved the spectral resolution in photoelectron spectra. The desired anions were then mass-selected by the TOF mass spectrometer before being photodetached by a laser beam in the detachment zone. Two different methods, *i.e.* magnetic-bottle TOF or VMI photoelectron spectrometers were used to collect and analyze the resultant photoelectrons detached by the lasers from the anions.

A. Magnetic-bottle TOF photoelectron energy analyzer

The selected APS^- ions were maximally decelerated after mass selection. Three photon energies were employed in the current study, 355 nm (3.496 eV) and 266 nm (4.661 eV) from a Nd:YAG laser, and 193 nm (6.424 eV) from an ArF excimer laser. All lasers were operated at a 20 Hz repetition rate with the ion beam off at alternating laser shots to enable shot-to-shot background subtraction to be carried out. Photoelectrons were collected at ∼100% efficiency with the magnetic bottle and analyzed in a 5.2 m long electron flight tube. The recorded TOF photoelectron spectrum was converted into an eKE spectrum by calibration with the known NIPE spectra of I^- [31] and $OsCl_6{}^{2-}$ [32]. The electron binding energy (EBE) was obtained by subtracting the electron kinetic energy from the energy of the detaching photons. The energy resolution was about 2% (*i.e.*, ∼20 meV for 1 eV kinetic-energy electrons).

B. VMI photoelectron spectroscopy

The selected anions reached the interaction imaging region without being decelerated, where they were photodetached by photons with three different wavelengths, *i.e.*, 440 nm (2.8178 eV), 450 nm (2.7552 eV), and 460 nm (2.6953 eV), from a Quanta-Ray MOPO-730 OPO/OPA laser pumped by a Quanta-Ray PRO 270 laser. Photoelectrons were focused with a VMI electrostatic lens onto a detector that is comprised of two chevron-stacked micro-channel plates coupled to a phosphor screen, and recorded with a CCD camera. The photoelectron-energy spectra were reconstructed from the accumulated images using the maximum-entropy velocity Legendre reconstruction (MEVELER) methods [33]. The spectrometer was calibrated with the well-characterized photodetachment transitions of PhS^- [34], Br^- [35], and I^- [31].

III. THEORETICAL METHODS

The geometries of APS^- and $APS^\bullet$ were optimized using density functional theory employing the B3LYP functional [36, 37], and the standard Pople type 6-31++G(d,p) [38] basis set for all the atoms, with the reported crystal structure crystal structure of related compounds [16] as the basis for the initial guess. Harmonic vibrational frequency analyses were carried out to confirm that the optimized structures were real minima. To evaluate the suitability of the B3LYP/6-31++G(d,p) method, the APS^- and $APS^\bullet$ structures were also optimized at the ωB97XD/aug-cc-pVTZ level

DOI:10.1063/1674-0068/31/cjcp1805114

[39], which yielded consistent results. The Gaussian 09 suite of programs [40] was used for geometry optimizations. Theoretical vertical detachment energy (VDE) for APS^- was calculated as the electronic energy difference between the neutral and anion both at the anion geometry. Theoretical adiabatic detachment energy (ADE) for APS^-, equivalent to the EA of neutral $APS^•$, was calculated as the electronic energy plus zero-point vibrational energy difference between the neutral and anion at each respective optimized geometry.

The Franck-Condon factors (FCFs) that were necessary in order to simulate the vibrational progressions in the NIPE spectra were computed with the ezSpectrum program [41]. However, it is unrealistic to do a full FC simulation by considering all of the $APS^•$ 72 fundamental vibration modes, their combination bands and overtones, due to the limited computer memory. Therefore only ten vibrational modes that yield the strongest FC intensities for the 0−1 transitions were selected in the input file to the ezSpectrum program for calculating the vibrational structures; the remaining 62 modes with orders of magnitude weaker FCFs were excluded in the simulations. In addition, the NWChem [42] suite of codes was used to calculate the dipole-bound electron orbitals, using the B3LYP exchange-correlation functional and by adding the diffuse set of functions of aug-cc-pV5Z to the positive side of the dipole moment [42–44].

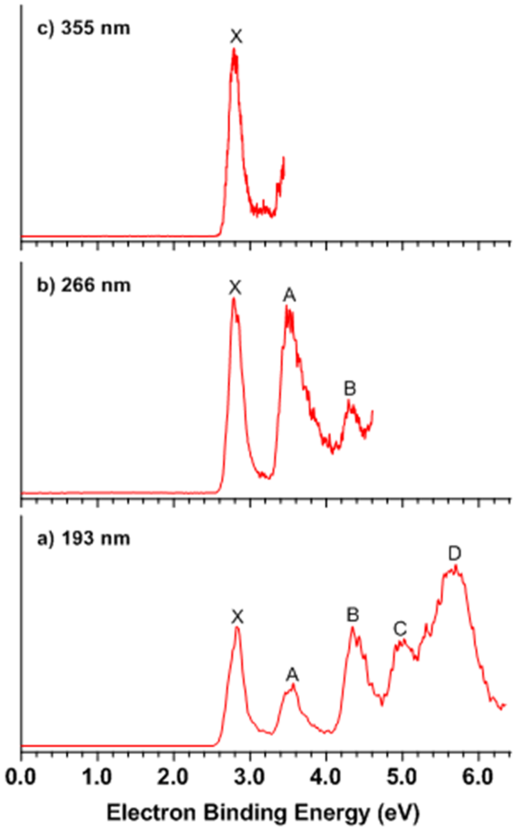

FIG. 1 The 20 K NIPE spectra of APS^- at (a) 193 nm, (b) 266 nm, and (c) 355 nm, respectively.

IV. EXPERIMENTAL RESULTS AND DISCUSSION

A. NIPE spectra of APS^-

FIG. 1 shows the 20 K NIPE spectra of APS^- recorded with 355, 266, and 193 nm lasers. The 193 nm spectrum (FIG. 1(a)) reveals five spectral features, labeled X, A, B, C, and D in the order of increasing EBE centered at EBE=2.8, 3.6, 4.4, 5.0, and 5.7 eV, respectively. These multiple spectral bands represent the electronic transitions from the ground state of the APS^- anion to the electronic ground (X) and excited states (A, B, C, and D) of the $APS^•$ neutral with respective associated vibrational excitations. At 266 nm (FIG. 1(b)), only the first three bands show up due to the photon energy limit of 266 nm, with reduced intensity for feature B. In the 355 nm spectrum (FIG. 1(c)), only band X and the onset of band A are observed. The experimental VDE of APS^-, measured from the band X maximum in the 355 nm spectrum, is (2.80±0.05) eV, which is confirmed (within experimental uncertainty) from the 266 nm and 193 nm spectra. Since no vibrational features were resolved in the spectrum, the experimental ADE was estimated by drawing a straight line along the leading edge of the X band and then adding the instrumental resolution (fwhm) to the EBE at the crossing point between the line and the EBE axis, to be 2.6 eV. In order to get a more accurate ADE, or equivalently, the EA of $APS^•$, we employed VMI PES which has higher resolution for slow photoelectrons (see the next section).

B. VMI photoelectron images of APS^-

FIG. 2 shows the 20 K VMI photoelectron spectra plotted in eKE (left) and images (right) of APS^-, recorded at 440, 450, and 460 nm, respectively. The VMI spectra have better resolution for slow electrons, showing vibrational fine structures. The ADE of APS^-, determined from the 0−0 transition with the highest eKE (blue downward arrows in FIG. 2), is (2.62±0.05) eV (Table I). Interestingly, the VMI spectra and images are dominant with an outstanding feature (*), observed with the same eKE=0.0179 eV for all three different wavelengths. The origin of this strong and sharp feature will be explained in the next sections.

V. THEORETICAL RESULTS AND DISCUSSION

Quantum chemical calculations were carried out, in order to obtain the optimized anion and neutral geometries, to calculate ADE/VDE of APS^- in comparing with the experimental values, and to compute the permanent dipole moment of $APS^•$. The FC simulations

DOI:10.1063/1674-0068/31/cjcp1805114

TABLE I Experimental and calculated adiabatic/vertical detachment energies (ADE/VDE) of APS^-, and the computed permanent dipole moment of $APS^\bullet$.

APS^-	Calculation[a]		Experiment
	B3LYP/6-31++G(d,p)	ωB97XD/aug-cc-pVTZ	
ADE/eV	2.51	2.48	2.62±0.05
VDE/eV	2.65	2.66	2.80±0.05
Neutral dipole moment/Debye	3.31	3.25	

[a] Spin-obit coupling is not included.

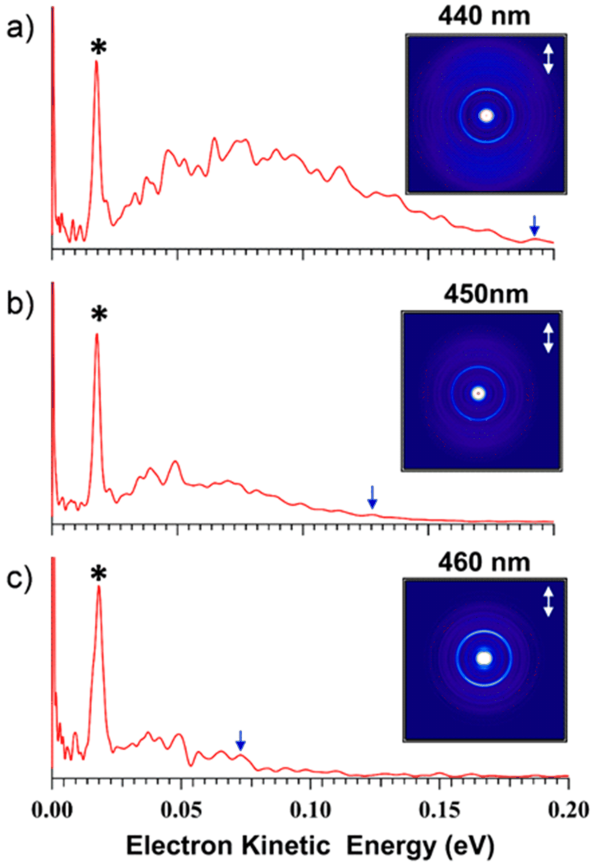

FIG. 2 The 20 K VMI photoelectron spectra (left) and images (right) of APS^- recorded with (a) 440 nm, (b) 450 nm, and (c) 460 nm lasers. The sharp peak (*) at eKE=17.9 meV comes from autodetachment through an anion dipole-bound state, in which each laser wavelength is in resonance with a specific vibrational level in the dipole-bound state (see FIG. 5). The 0-0 position, from which the experimental ADE is measured, is indicated with the blue downward arrows, and the polarization of laser is shown with the white double arrows.

for the spectrum including spin-orbit coupling (SOC) effects were further conducted to understand the spectral profile and to have a direct comparison between the simulated and experimental spectra. In addition, schematic energy diagram (FIG. 5) and dipole-bound electron orbitals are invoked in explaining the observed

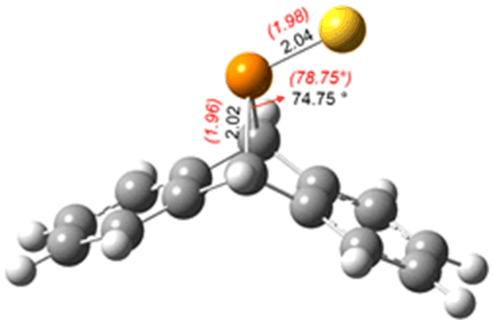

FIG. 3 Optimized structures of APS^- and $APS^\bullet$ with the key bond lengths (Å) and bond angles (°) noted (numbers in black plain text for APS^-, and those in red italic inside parenthesis for $APS^\bullet$) (H: light grey, C: dark gray, P: orange, S: yellow).

autodetachment channels.

A. Optimized geometries of $APS^{-/\bullet}$ and calculated ADE/VDE

FIG. 3 shows the optimized structures with the key bond lengths and bond angles noted for both APS^- and $APS^\bullet$. (Additional metrical data such as the B3LYP (X, Y, Z) coordinates are listed in Table S1 in the supplementary materials). Our calculations show that the isolated APS^- anion has a C_s symmetry and overall similar structure to other known RPA compounds [16, 18–20]. It features a strained architecture at the phosphorus center, with an acute C(21)−P(22)−C(24) angle of 74.75° and P(22)−C(21/24) bond lengths of 2.02 Å. The corresponding neutral $APS^\bullet$ structure was also optimized and is compared with the anion in FIG. 3, revealing overall minor geometric changes upon the electron detachment. However, the neutral $APS^\bullet$ has a significantly wider C−P−C angle (78.75°) and two slightly shortened P−C bonds (1.96 Å) compared to those in the anion. In addition, the P(22)−S(23) distance decreases by 0.06 Å and the C(21)−C(24)−P(22)−S(23) dihedral angle increased by 11.74°, upon one electron detachment. The key bond lengths and bond angles obtained for the neutral $APS^\bullet$ are almost identical to a typical RPA compound with C−P−C angle of 79° and P−C bonds of 1.91 Å [16]. The B3LYP/6-31++G(d,p)

DOI:10.1063/1674-0068/31/cjcp1805114

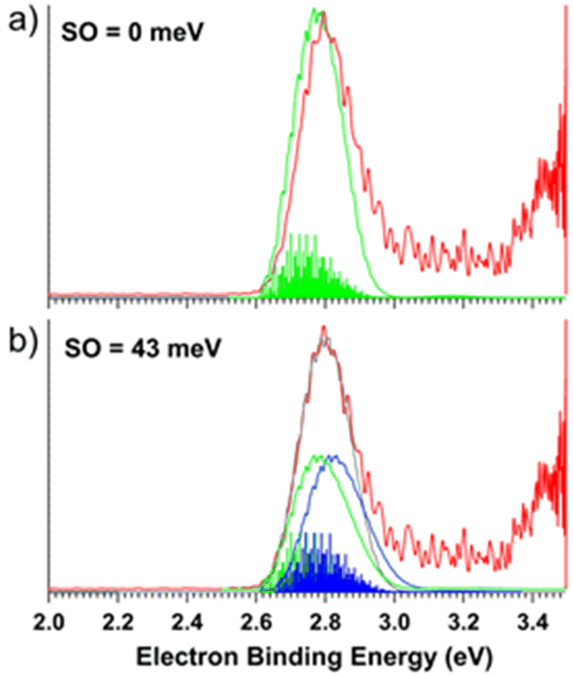

FIG. 4 (a) The simulated spectrum (green) of APS^- without considering SO splitting, superimposed onto the experimental 355 nm spectrum (red); (b) The simulated spectrum (grey) summed from the two sets of identical green and blue spectra, separated by a SO=43 meV splitting, superimposed onto the experimental one (red). The Gaussian 09 suite of programs [40] was used for geometry optimizations and frequency calculations.

and ωB97XD/aug-cc-pVTZ calculated ADE/VDE, *i.e.*, 2.51/2.65 eV for the former, and 2.48/2.66 eV for the latter, are both slightly smaller than the corresponding experimental values of 2.62/2.80 eV (Table I).

B. Simulated NIPE spectra for APS^-

The relatively large size of the $APS^{-/\bullet}$ molecule makes full FC simulations unfeasible, in which all of its 72 fundamental vibration modes, and their combination, overtone bands would have been included. Therefore only vibrational normal modes that yield the strongest 0-1 FCFs are selected and included in the final neutral target state (total ten modes). All of the remaining modes are found to have much weaker 0-1 FCFs (orders of magnitude weaker) and are excluded in the FC simulation. FIG. 4(a) shows the simulated 355 nm spectrum for formation of the ground state of $APS^\bullet$, using the calculated B3LYP/6-31++G(d,p) stick spectrum, convoluted with Gaussian line broadening with full width at half maximum (FWHM) of 10 meV for the sticks. However, the simulated spectrum (green) shows an obviously steeper rising edge compared with the experimental spectrum (red), which is superimposed for direct comparison.

The spectral band in FIG. 4 represents the transition from the ground state of APS^- — a closed-shell anion, to the ground state of $APS^\bullet$ — an open-shell neutral radical with one unpaired electron. Therefore spin orbit coupling (SOC) should be considered in the final neutral state. Recently we reported a SO=(37±2) meV for $PCS^\bullet$ measured from the observed NIPE spectra of PCS^- [30], a value that is in excellent agreement with the calculated SO=36 meV by our group [30] and 39.5 meV by Peterson *et al.* [45]. In addition, an experimental SO splitting of $PS^\bullet$, measured from the J=1/2 and 3/2 components in the ground state, was reported to be ∼40 meV [25].

In the current $APS^\bullet$ case, it is not possible for us to experimentally determine the SO splitting, because too many atoms and vibrational modes are involved. Instead we invoke FC simulations by including SOC in the simulated spectrum to see if we can have a better agreement with the experiments. FIG. 4(b) shows a simulated NIPE spectrum summed from two sets of identical FC stick spectra (the same spectrum as in FIG. 4(a)) with a SO=43 meV separated between them. It can be seen that including SOC in the simulation significantly improves the simulated spectrum compared to the experimental one. The simulation also pinned down the 0−0 transition in the spectrum of APS^-, leading to EA=2.62 eV for $APS^\bullet$, consistent with the EA determined from VMI spectra in FIG. 2. Additional simulations with slightly different SO splittings were conducted and presented in FIG. S3 in the supplementary materials for this manuscript. Among all of the simulations, the one with SO=43 meV in FIG. 4 agrees best with experiments both in terms of peak positions and intensities. The successful simulation of the APS^- spectrum in FIG. 4 provides further credence for the optimized B3LYP structures.

C. Dipole-bound state (DBS)

Polar molecules can attract an excess electron, creating what is known as a dipole-bound anion [46]. As previously reported, NIPES has become an effective method to probe dipole bound state through observing spectroscopic signatures with strong and sharp peaks at a rather low EBE for species with sufficient dipole moment (>2.5 D) [46–49]. Our calculations from the B3LYP/6-31++G(d,p) level show that the $APS^\bullet$ neutral has a dipole moment of 3.31 Debye which is significantly capable of supporting a DBS. The vibrational frequencies in a DBS are similar to those of the neutral molecule, and the autodetachment from the DBS vibrational levels to the corresponding neutral vibrational levels obeys the $\Delta v = v_{\text{neutral}} - v_{\text{anion}} = -1$ propensity rule [50, 51]. Hence autodetachment from the excited DBS of APS^- to the nearest vibrational level of the neutral $APS^\bullet$ can generate outgoing electrons with the same kinetic energy (17.9 meV) from different

DOI:10.1063/1674-0068/31/cjcp1805114

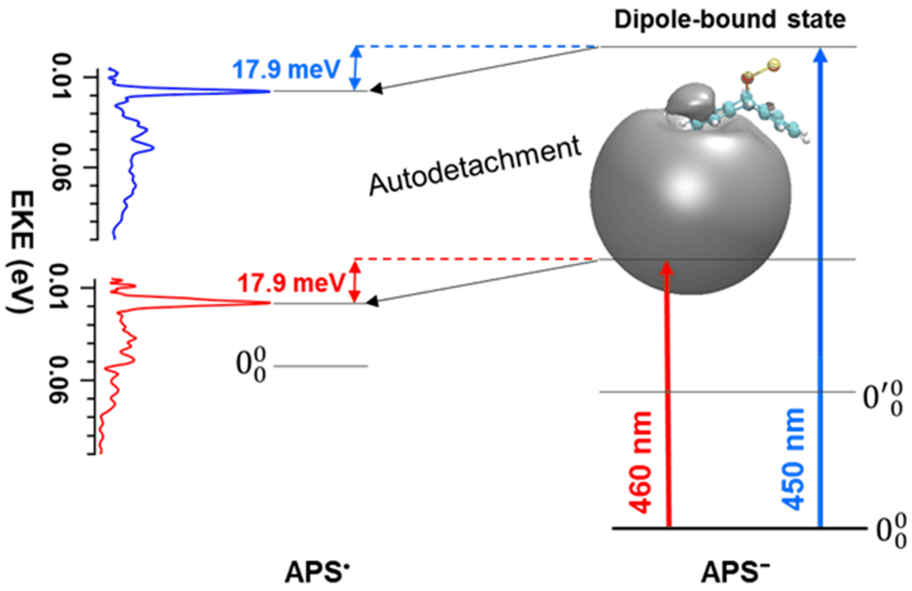

FIG. 5 Schematic energy diagram showing transitions from the ground state of APS^- to the excited dipole-bound states (DBSs) and associated autodetachment to $APS^\bullet$ neutral. The $0'^0_0$ represents the ground vibration level of the DBS.

starting vibrational states, resulting in the same radius rings in three imaging spectra at different wavelengths (440, 450, and 460 nm) as experimentally observed in FIG. 2. The schematic energy diagram showing transitions from the ground state of APS^- to the excited DBSs and associated autodetachment to the $APS^\bullet$ neutral is drawn out in FIG. 5 to illustrate the autodetachment processes described above. The photoelectron angular distribution information obtained from the images also gives additional qualitative evidence of the autodetachment. The sharp peaks with 17.9 meV kinetic energy are nearly isotropic (β=0.09, 0.18, and 0.24 for 440, 450, and 460 nm, respectively). Due to the complexity of the APS^- molecule and numerous possible combination frequencies, assignments of specific transitions related to the experimental results are not attempted here. Nevertheless, a brief analysis of the eKE=17.9 meV=144 cm^{-1} peak observed at 440, 450, and 460 nm gives rise to a provisional, self-consistent assignment (FIG. S3 in supplementary materials), corresponding to the Δv_8=−1 vibrational transition (the inter-wobbling motion between the two benzo rings with a frequency of 302 cm^{-1}, FIG. S4 in supplementary materials), which, in turn, yields that the ground vibrational state of $APS^\bullet$ is 302−144=158 cm^{-1} above the ground vibrational state of DBS of APS^- (FIG. S3 in supplementary materials). As the excess dipole bound electron is very diffuse and weakly bound with the molecule, detaching it marginally changes the molecular structure. The dipole bound electron orbital, obtained with adding the aug-cc-pV5Z basis set to the positive side of dipole moment using the structure of the neutral $APS^\bullet$, is shown in FIG. 5.

VI. CONCLUSION

In summary, we report a joint NIPES, VMI PES and quantum chemical study of the dibenzo-7-phosphanorbornadiene P-sulfide anion APS^- and its neutral radical $APS^\bullet$. The EA and SO splitting of the $APS^\bullet$ neutral is determined to be (2.62±0.05) eV and (43±7) meV, respectively. VMI photoelectron images show a strong and sharp ring with the same radius in three imaging spectra, taken at three different wavelengths, that is originated from autodetachment from dipole-bound states of the APS^- anion. The B3LYP/6-31++G(d,p) and ωB97XD/aug-cc-pVTZ calculations show that the $APS^\bullet$ neutral has a dipole moment of 3.31 and 3.25 Debye, which is significantly capable of supporting a DBS. The intrinsic molecular properties of APS^- and $APS^\bullet$, obtained in this work, may help better understand its transformation and reactivity in various chemical and biochemical environments.

Supplementary materials: Bond lengths (Å) and bond angles (°) of $APS^{-/\bullet}$ (Table S1); optimized structures of APS^- with all atom being labeled (FIG. S1), simulated spectra of $APS^\bullet$ without SO splitting, simulated spectra of $APS^\bullet$ with different SO splitting spaces (FIG. S2), a possible transition schematic to explain the sharp peak with 144 cm^{-1} eKE at different wavelengths (FIG. S3), vibrational mode #8 of the neutral $APS^\bullet$(FIG. S4), and Cartesian coordinates for the optimized structures of $APS^{-/\bullet}$ are available.

VII. ACKNOWLEDGEMENTS

The work was supported by the U.S. Department of Energy (DOE), Office of Science, Office of Basic Energy

DOI:10.1063/1674-0068/31/cjcp1805114

Sciences, Division of Chemical Sciences, Geosciences and Biosciences, and was performed using EMSL, a national scientific user facility sponsored by DOE's Office of Biological and Environmental Research and located at Pacific Northwest National Laboratory, which is operated by Battelle Memorial Institute for the DOE. The experimental work conducted at MIT was supported by the National Science Foundation under Grant (No.CHE-1664799).

[1] I. Krummenacher and C. C. Cummins, Polyhedron **32**, 10 (2012).
[2] F. F. Puschmann, D. Stein, D. Heift, C. Hendriksen, Z. A. Gal, H. F. Grützmacher, and H. Grtzmacher, Angew. Chem. Int. Ed. **50**, 8420 (2011).
[3] A. R. Jupp and J. M. Goicoechea, Angew. Chem. Int. Ed. **52**, 10064 (2013).
[4] A. M. Tondreau, Z. Benkő, J. R. Harmer, and H. Grützmacher, Chem. Sci. **5**, 1545 (2014).
[5] D. Heift, Z. Benkő, H. Grützmacher, A. R. Jupp, and J. M. Goicoechea, Chem. Sci. **6**, 4017 (2015).
[6] A. R. Jupp and J. M. Goicoechea, J. Am. Chem. Soc. **135**, 19131 (2013).
[7] A. R. Jupp, G. Trott, É. Payen de la Garanderie, J. D. Holl, D. Carmichael, and J. M. Goicoechea, Chem. Eur. J. **21**, 8015 (2015).
[8] A. Hinz, R. Labbow, C. Rennick, A. Schulz, and J. M. Goicoechea, Angew. Chem. Int. Ed. **56**, 3911 (2017).
[9] D. Heift, Z. Benkő, and H. Grützmacher, Chem. Eur. J. **20**, 11326 (2014).
[10] D. Heift, Z. Benkő, and H. Grützmacher, Dalton Trans. **43**, 831 (2014).
[11] X. Chen, S. Alidori, F. F. Puschmann, G. Santiso-Quinones, Z. Benkő, Z. Li, G. Becker, H. F. Grützmacher, and H. Grützmacher, Angew. Chem. Int. Ed. **53**, 1641 (2014).
[12] T. P. Robinson and J. M. Goicoechea, Chem. Eur. J. **21**, 5727 (2015).
[13] K. Nakajima, W. Liang, and Y. Nishibayashi, Org. Lett. **18**, 5006 (2016).
[14] Christian Hering-Junghans and Eric Rivard, Angew. Chem. Int. Ed. **54**, 10077 (2015).
[15] A. Velian and C. C. Cummins, Science **348**, 1001 (2015).
[16] A. Velian and C. C. Cummins, J. Am. Chem. Soc. **134**, 13978 (2012).
[17] A. Velian, M. Nava, M. Temprado, Y. Zhou, R. W. Field, and C. C. Cummins, J. Am. Chem. Soc. **136**, 13586 (2014).
[18] A. Velian, W. J. Transue, and C. C. Cummins, Organometallics **34**, 4644 (2015).
[19] W. J. Transue, A. Velian, M. Nava, M. A. Martin-Drumel, C. C. Womack, J. Jiang, G. L. Hou, X. B. Wang, M. C. McCarthy, and R. W. Field, J. Am. Chem. Soc. **138**, 6731 (2016).
[20] W. J. Transue, A. Velian, M. Nava, C. García-Iriepa, M. Temprado, and C. C. Cummins, J. Am. Chem. Soc. **139**, 10822 (2017).
[21] G. L. Hou, B. Chen, W. J. Transue, D. A. Hrovat, C. C. Cummins, W. T. Borden, and X. B. Wang, J. Phys. Chem. A **120**, 6228 (2016).
[22] G. L. Hou, B. Chen, W. J. Transue, D. A. Hrovat, C. C. Cummins, W. T. Borden, and X. B. Wang, Chem. Sci. **7**, 4667 (2016).
[23] C. Visscher, K. Lodders, and B. Fegley Jr., Astrophys. J. **648**, 1181 (2006).
[24] S. B. Yaghlane, J. S. Francisco, and M. Hochlaf, J. Chem. Phys. **136**, 244309 (2012).
[25] K. Dressler and E. Miescher, Proc. Phys. Soc. Sect. A **68**, 542 (1955).
[26] N. Narasimham and T. Subramanian, J. Mol. Spectrosc. **29**, 294 (1969).
[27] Z. Mielke, G. D. Brabson, and L. Andrews, J. Phys. Chem. **95**, 75 (1991).
[28] C. Xu, E. de Beer, and D. M. Neumark, J. Chem. Phys. **104**, 2749 (1996).
[29] X. B. Wang and L. S. Wang, Rev. Sci. Instrum. **79**, 073108 (2008).
[30] G. L. Hou, B. Chen, W. J. Transue, Z. Yang, H. R. Grützmacher, M. Driess, C. C. Cummins, W. T. Borden, and X. B. Wang, J. Am. Chem. Soc. **139**, 8922 (2017).
[31] D. Hanstorp and M. Gustafsson, J. Phys. B: At. Mol. Opt. Phys. **25**, 1773 (1992).
[32] X. B. Wang and L. S. Wang, J. Chem. Phys. **111**, 4497 (1999).
[33] B. Dick, Phys. Chem. Chem. Phys. **16**, 570 (2014).
[34] J. B. Kim, T. I. Yacovitch, C. Hock, and D. M. Neumark, Phys. Chem. Chem. Phys. **13**, 17378 (2011).
[35] C. Blondel, P. Cacciani, C. Delsart, and R. Trainham, Phys. Rev. A **40**, 3698 (1989).
[36] A. D. Becke, Phys. Rev. A **38**, 3098 (1988).
[37] A. D. Becke, J. Chem. Phys. **98**, 5648 (1993).
[38] G. Petersson and M. A. Al-Laham, J. Chem. Phys. **94**, 6081 (1991).
[39] J. D. Chai and M. Head-Gordon, Phys. Chem. Chem. Phys. **10**, 6615 (2008).
[40] M. J. Frisch, G. W. Trucks, H. B. Schlegel, G. E. Scuseria, M. A. Robb, J. R. Cheeseman, G. Scalmani, V. Barone, B. Mennucci, G. A. Petersson, H. Nakatsuji, M. Caricato, X. Li, H. P. Hratchian, A. F. Izmaylov, J. Bloino, G. Zheng, J. L. Sonnenberg, M. Hada, M. Ehara, K. Toyota, R. Fukuda, J. Hasegawa, M. Ishida, T. Nakajima, Y. Honda, O. Kitao, H. Nakai, T. Vreven, J. A. Montgomery, J. E. Peralta, F. Ogliaro, M. Bearpark, J. J. Heyd, E. Brothers, K. N. Kudin, V. N. Staroverov, R. Kobayashi, J. Normand, K. Raghavachari, A. Rendell, J. C. Burant, S. S. Iyengar, J. Tomasi, M. Cossi, N. Rega, J. M. Millam, M. Klene, J. E. Knox, J. B. Cross, V. Bakken, C. Adamo, J. Jaramillo, R. Gomperts, R. E. Stratmann, O. Yazyev, A. J. Austin, R. Cammi, C. Pomelli, J. W. Ochterski, R. L. Martin, K. Morokuma, V. G. Zakrzewski, G. A. Voth, P. Salvador, J. J. Dannenberg, S. Dapprich, A. D. Daniels, Farkas, J. B. Foresman, J. V. Ortiz, J. Cioslowski, and D. J. Fox, *Gaussian 09, Revision A02*, Wallingford, CT: Gaussian Inc., (2009)
[41] V. A. Mozhayskiy and A. I. Krylov, *ezSpectrum, version 3.0*, Los Angeles: University of Southern alifornia. http://iopenshell.usc.edu/downloads.
[42] M. Valiev, E. J. Bylaska, N. Govind, K. Kowalski, T.

DOI:10.1063/1674-0068/31/cjcp1805114

P. Straatsma, H. J. Van Dam, D. Wang, J. Nieplocha, E. Apra, and T. L. Windus, Comput. Phys. Commun. **181**, 1477 (2010).
[43] T. H. Dunning Jr., J. Chem. Phys. **90**, 1007 (1989).
[44] D. E. Woon and T. H. Dunning Jr., J. Chem. Phys. **98**, 1358 (1993).
[45] B. Finney, A. O. Mitrushchenkov, J. S. Francisco, and K. A. Peterson, J. Chem. Phys. **145**, 224303 (2016).
[46] O. H. Crawford, Mol. Phys. **20**, 585 (1971).
[47] C. Desfrançois, H. Abdoul-Carime, and J. P. Schermann, Int. J. Mod. Phys. B **10**, 1339 (1996).
[48] J. H. Hendricks, H. L. de Clercq, S. A. Lyapustina, and K. H. Bowen Jr., J. Chem. Phys. **107**, 2962 (1997).
[49] A. Buytendyk, A. Buonaugurio, S. J. Xu, J. Nilles, K. Bowen, N. Kirnosov, and L. Adamowicz, J. Chem. Phys. **145**, 024301 (2016).
[50] J. Simons, J. Am. Chem. Soc. **103**, 3971 (1981).
[51] H. T. Liu, C. G. Ning, D. L. Huang, P. D. Dau, and L. S. Wang, Angew. Chem. Int. Ed. **125**, 9146 (2013).

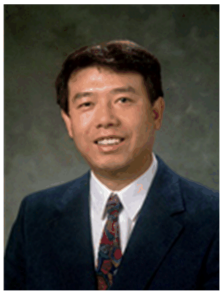

Xue-Bin Wang received his B.S. in Chemical Physics from University of Science and Technology of China (1988) and his Ph.D in Physical Chemistry from the Institute of Chemistry, Chinese Academy of Sciences (1995) under the supervision of Qi-he Zhu. He worked as a visiting graduate student under the guidance of R. D. Levine from 1993 to 1995 in Hebrew University of Jerusalem. He Joined R. Bersohn's group in 1995 at Columbia University, and L. S. Wang's group in 1997 at PNNL/Washington State University as a postdoctoral Research associate. He worked at PNNL/Washington State University as a research scientist and an associate research professor from 2000 to 2011. He formally joined PNNL in 2011 and is currently a senior research scientist in the Physical Sciences Division at PNNL. He was elected to be a Fellow of the American Physical Society (APS) in 2016. His scientific interests focus on cluster model study of condensed phase chemistry and phenomena via combined photoelectron spectroscopy and theoretical approach.

DOI:10.1063/1674-0068/31/cjcp1805114